Photoinduced phenomena in amorphous Se: overview and notions

K. TANAKA*
Department of Applied Physics, Graduate School of Engineering, Hokkaido University, Sapporo, Japan

Amorphous chalcogenide semiconductors exhibit a variety of light-induced phenomena, such as darkening, fluidity, deformation, crystallization, and phase change, some of which appear anisotropically upon illumination of linearly-polarized light. For studying these phenomena, Se may be the most suitable, since its microscopic structure is simple, being composed with entangled chains consisting of only homopolar bonds. Hence, after briefly reviewing light-induced changes in Se, including the phase change, we explore relationships between photodarkening and photo-crystallization, using a configurational diagram. Roles of athermal and thermal effects are quantitatively discussed. Besides, a model for understanding unique features of the anisotropic deformations is proposed.

(Received October 19, 2021; accepted February 11, 2022)

Keywords: Selenium, Chalcogenide, Photodarkening, Photo-crystallization, Phase change, Anisotropy

1. Introduction

It is known that amorphous chalcogenide materials exhibit many kinds of photoinduced phenomena, for which mechanisms and applications have been studied over a half century [1-4]. Among such phenomena, the most successfully utilized is undoubtedly the optical phase change in Te-compound films, the mechanism being understood principally through opto-thermally induced processes. It is also known that S compounds such as As_2S_3 undergo non-thermal, photoinduced atomic transformations, a representative being photodarkening. And, a-Se exhibits both thermal and non-thermal changes. Besides, the elemental structure consisting of entangled chains [5-7] possesses no compositional disorder, which could make Se the most appropriate material for exploring fundamental mechanisms of the light-induced phenomena.

Hence, we briefly review known phenomena in Se [1-4, 7], including optical phase changes [8]. We also characterize two scalar phenomena, photodarkening and photo-crystallization, which are efficiently induced by geminate and free carriers, using a configuration-coordinate diagram. Finally, it is proposed that vector changes arise from two-dimensional, disordered, segmental Se chains.

2. Known light-induced phenomena

Table 1 lists light-induced phenomena in a-Se films, which are prepared with evaporation on to substrates held at room temperature or ~50°C. Besides, some are observable also in bulk samples [9, 10]. Since the phenomena are diverse, the table classifies those into several groups, with (speculated) structural changes; local/defective, non-local/extended, crystallization, and phase change. In addition, some exhibit isotropic (scalar) and anisotropic (vector) changes, upon illumination of linearly-polarized light. However, the table excludes phenomena which affect photoluminescence and ESR properties at cryogenic temperatures [4, 11, 12]. It also excludes photoinduced changes appearing in red a-Se films, which could be prepared by deposition on to cooled substrates. The film may undergo photo-polymerization upon illumination at room temperature [13, 14]. The present work also excludes interesting phenomena appearing in liquid Se, for which comprehensive studies have been performed by Sakaguchi and Tamura [2, 15].

Table 1. Known light-induced changes in a-Se with related publications.

	Isotropic (Scalar)	Anisotropic (Vector)
Local / defective	Photodarkening [10, 16, 18, 19, 22-28]	Dichroism and birefringence [29-35]
Non-local / extended	Photo-fluidity [9, 20, 36-45] Photo-expansion [38, 46-48]	Vector deformation [48, 57-62]
Crystallization	Photo-crystallization [63-75, 78, 82]	Oriented crystallization [76-78]
Phase change	Phase change [8]	

2.1. Local / defective

Chang may be the first, who noticed a quasi-stable, scalar (polarization-independent) absorption increase in Se layers (a few mm thick) upon illumination of white light [10]. A successive study demonstrated, as shown in Fig. 1, that photodarkening (reversible redshifts ΔE of the optical absorption edge) with $\Delta E \leq 60$ meV appears in Se films at low (~80 K) temperatures [16]. Note that a similar change appears also in a-S films at ~80 K [17, 18]. Thus, these results manifest that the phenomenon occurs in elemental amorphous chalcogen having no compositional variations. The magnitude ΔE decreases with a temperature ratio T_i/T_g (= 0 ~ 1) and it becomes zero at $T_i/T_g \approx 1$ [16, 17], where T_i is the temperature at which a sample is illuminated and T_g (~310 K in Se) is the glass-transition temperature. Such temperature dependence suggests that no thermal energy is required for inducing the photodarkening, while it can be thermally recovered with annealing at T_g. And, the darkening mechanism has been ascribed to *enhanced structural disordering*, which can broaden the valence band consisting of lone-pair electron states of chalcogen [7, 19] through, e.g., atomic bond twisting [7, 17, 18] and/or coordination changes [20, 21]. Pressure studies support such an idea [18, 22, 23]. Transient characteristics have been studied in [24-28].

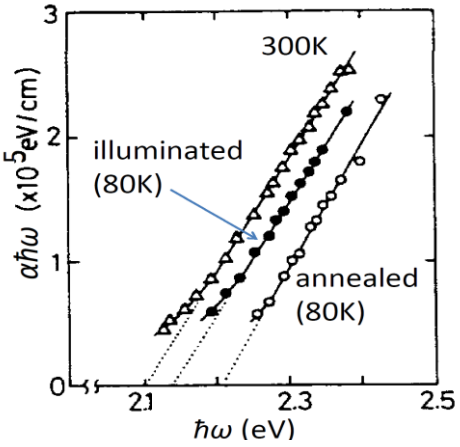

Fig. 1. Photodarkening (○, ●) in an a-Se film at 80 K, with no photoinduced effects (△) at 300 K [16]

Se exhibits also the so-called 'vector' changes, as reviewed [29, 30]. After the discovery by Zhdanov and Malinovskii [31] of quasi-stable optical anisotropy (dichroism and birefringence) induced by linearly-polarized light in As_2S_3, similar changes were uncovered for a-Se [32, 33]. The induced anisotropy in these materials is *negative*; e.g., $n(//E) < n(\perp E)$, where $n(//E, \perp E)$ denote refractive indices measured by probe light with an electric field parallel and perpendicular to that E of excitation light. It should also be underlined that, different from the photodarkening, the optical anisotropy in a-Se is efficiently induced at ~200 K [33]. Such an observation is consistent with Fritzsche's phenomenological model for the photoinduced anisotropy [34, 35], which is discussed in Section 3.2, with atomic pictures of the anisotropic element.

2.2. Non-local / extended

About a century ago, Vonwiller noticed an anomalous photoinduced mechanical change [9]. Se samples exposed to light illumination became soft, which was later referred to as photoinduced stress-relaxation [20, 36, 37], fluidity (viscosity) [38-40], or photo-melting [41-43]. A similar phenomenon in As_2S_3 demonstrates that the fluidity occurs athermally [44], for which the author envisages a mechanism as domino-like, relaxational slippage of chain (layer) molecules through bond interchanges [26, 40, 45].

Se exhibits volume expansion at room temperature, at which little photodarkening occurs as shown in Fig. 1 [16]. The expansion appears transitory during illumination [46, 47], which may be retained in quasi-stable after its termination [38, 48-51]. It is plausible that the local structural change giving rise to the photodarkening is transformed through photoinduced fluidity to the macroscopic shape change [26], and accordingly, it remains quasi-stable at room temperature. We also know that the photo-expansion in As_2S_3 becomes greater at lower temperatures [51], which would suggest a similar temperature variation for Se. Theoretical studies demonstrate that the expansion is triggered with structural disordering induced by photo-generated *electrons* [52-54].

On the other hand, at least three kinds of vector (anisotropic) deformations appear upon illumination of a linearly-polarized light beam [45, 55]. Regarding so-called M-shape deformation in thin films [56] and an opto-mechanical effect in bilayer cantilevers [57], Se undergoes qualitatively the same behaviours to those in As_2S_3 [45, 48]. By contrast, photoinduced elongations in Se and $As_2S(Se)_3$ samples on viscous substrates exhibit contrastive behaviours [45, 55, 58]. Upon illumination of linearly-polarized light, $As_2S(Se)_3$ elongate 'orthogonal' to the electric filed [45, 55, 59, 60], which could be triggered by optical forces of scattered light [55, 61]. By contrast, as shown in Fig. 2, small (~10 μm) Se flakes laid on viscous grease elongate in the direction 'parallel' to the electric vector [55, 58, 60], with sample rotation, which may reflect optical torque [55]. It should be mentioned that exposures with holographic arrangements add much more varieties in appearance [38, 49, 50], the mechanisms being studied from different viewpoints [45, 62].

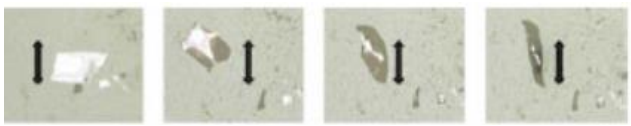

Fig. 2. Deformation of Se flakes with a thickness of ~1.5 μm on grease induced by illumination of semiconductor-laser light (1.8 eV and 20 mW) with exposure times of 0, 8, 27, 46 h (from left to right) [55]. The arrow indicates direction of the electric field, the length being 10 μm (color online)

2.3. Crystallization

Light-induced crystallization in a-Se, comprehensively studied by Dresner and Stringfellow [63], is a known phenomenon. They observed using an optical microscope that a crystallization speed of a-Se films held at ~50°C can be enhanced up to an order with illumination of cw light emitted from a 200 W Hg arc. As known, the crystallization proceeds through nucleation and growth, and they uncovered that the *growth* of pre-existing nuclei is enhanced by photo-generated *holes*. It seems that the hole assists cooperative, extended chain alignment, which is consistent with theoretical analyses that suggest, not electrons, but holes are responsible for chain alignments [52-54].

The photo-crystallization appears promising to some applications such as image memories [64, 65]. The crystallization occurs also upon excitation of fs-pulses at room temperature [66, 67], which may be utilized in nano-fabrications. The fs-pulse crystallization could also be applied to the phase change (see, Section 2.4).

However, the crystallization is problematic in photoconductive applications, which motivates considerable investigations. Besides, the crystallization rate has now been inspected using Raman-scattering spectroscopy with higher sensitivity [68, 69]. Such studies revealed an unexpected feature, as shown by the dotted lines in Fig. 3 [70 - 72]; in contrast to the observation of the light-induced crystallization above T_g (~ 310 K) [63], the crystallization under intense (~17 W/cm^2) He-Ne laser ($\hbar\omega \approx E_g$) illumination emerges at the temperature range of 260 – 340 K; except at around T_g, which is ascribable to structural relaxation that suppresses nuclei growth. Besides, Lindberg et al. confirmed that in Se films on soft substrates the crystallization tends to be suppressed [72], which suggests that local strain affects the photo-crystallization [70, 71]. Nonetheless, it remains unclear whether the effect is directly structural [73] and/or it just enhances electronic excitation efficiency through reducing local optical gap energy [40, 54]. Recent studies also manifest unknown aspects of the crystallization [74, 75].

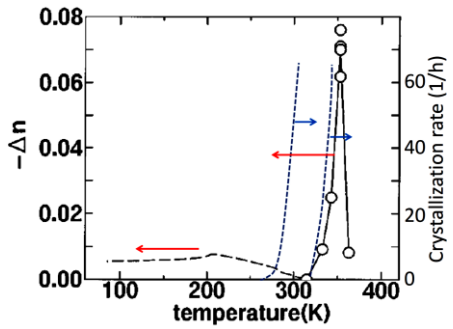

Fig. 3. Temperature variations of photoinduced birefringence [33, 76] (dashed and solid lines with the left-hand side axis) and photo-crystallization rate (the inverse of crystallization onset time) [70-72] (dotted lines with the right-hand side axis) (color online)

Se also exhibits a vector crystallization phenomenon. As shown in Fig. 3, illumination with linearly-polarized light at ~350 K gives rise to birefringence of ~0.1 [76, 77], which is greater by an order than that [33] induced in amorphous states. X-ray, Raman-scattering and microscope inspections unambiguously demonstrate oriented crystallization of Se chains [76-78], which manifests that the photoinduced crystallization could become macroscopically anisotropic upon illumination of linearly-polarized light. Note that, at higher temperatures than ~360 K, thermal crystallization prevails.

2.4. Phase change

As demonstrated by Hamanaka [8], Se undergoes the so-called optical phase change. He prepared 0.1 μm-thick a-Se films through evaporation on to collodion films, and illuminated a-Se with focussed light emitted from a He-Ne laser (λ = 633 nm). The sample probably has small heat capacity, which could be easily heated by illumination.

The irradiation effect is shown in Fig. 4a. We see that amorphous-to-crystalline transformation occurs upon an exposure with intensity of 0.5 mW/(5 μm)^2 (≈ 2 kW/cm^2) for 0.3 s, which corresponds to a dose of 600 J/cm^2. On the other hand, a crystalline-to-amorphous change occurs at

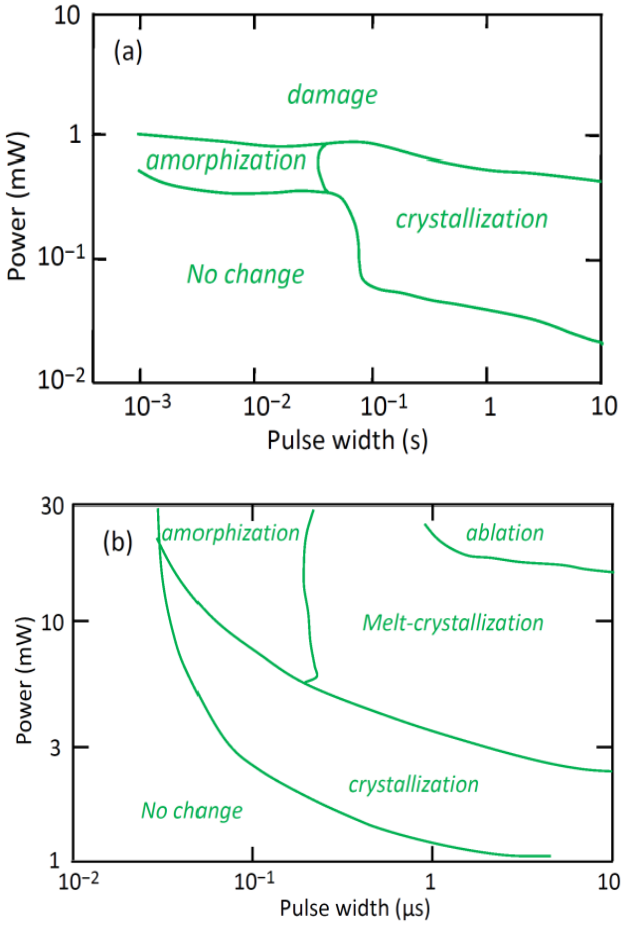

Fig. 4. Irradiation characteristics in (a) Se [8] and (b) $GeSb_2Te_4$ [79] (color online)

0.8 mW/(2 μm)^2 (= 20 kW/cm^2) for 1 ms, which gives 20 J/cm^2. (The light-spot sizes are estimated from printed photographs in [8].) Neglecting thermal dissipation, we may suppose $\Delta T = Q/c$ with a typical absorbed dose of Q = 10^2 J/cm^2 ×10^4 /cm = 10^6 J/cm^3 (with an absorption coefficient of 10^4 /cm) and the heat capacity of c = 1.4 J/cm^{3}K for Se [4], which leads to $\Delta T = 10^5$ K, being sufficient for the phase change. Note that *electrical* phase-changes in Se films have also been demonstrated [7].

Comparing the locations of the optical phase-change regions in Se [8] and $GeSb_2Te_4$ [79] in Fig. 4(a, b), we see marked differences. In $GeSb_2Te_4$ that is exposed to pulsed light (λ = 850 nm) with a power of I = 10 mW, crystallization occurs at ~50 ns, amorphization at ~100 ns, and melt-crystallization at ≥ 200 ns. In contrast, in a-Se, the 'crystallization' appears at higher doses than those for the amorphization. Since the crystalline-to-amorphous transformation needs the melting [4], the observed crystallization in a-Se appears to occur through melting, or it must be melt-crystallization, as observed in (b). No direct crystallization seems to be detected in Hamanaka's experiments. However, the photo-crystallization in a-Se under cw and pulsed excitations is a known phenomenon (Section 2.3), and accordingly, we speculate that Raman-scattering inspection could detect the phenomenon in the 'no-change region' in his result, which will be worthwhile exploring. On the other hand, in the two materials, the positional relationships between the amorphization and the melt-crystallization are qualitatively the same, with a conspicuous difference of the boundaries at the exposure time of 10^2 ms (a) and 10^2 ns (b), being different by six orders of magnitude. Such contrastive time-scales may reflect the scale of atomic motions for the melt-crystallizations in pure Se and the Te-compound.

3. Mechanisms

3.1. Photodarkening and crystallization

Having overviewed the photoinduced phenomena in a-Se, we consider the two, fundamental scalar phenomena; photodarkening and photo-crystallization. As known the photodarkening appears universally in covalent chalcogenide glasses and it is athermal, while the photo-crystallization is more-or-less unique to a-Se and thermally-activated [1-4].

The two phenomena can be grasped using an energy-configuration diagram, shown in Fig. 5. The configuration space consists of two axes q_1 and q_2, which represent intra- and inter-chain structures, and the energy in the vertical axis denotes the sum of electronic and lattice systems at 0 K. Needlessly, the intra- and inter-chain atomic motions are likely to couple, while we simply represent those with the two coordinates. The q_1-energy relation follows the single-and-double wells model previously proposed for As_2S_3 [17, 18, 80].

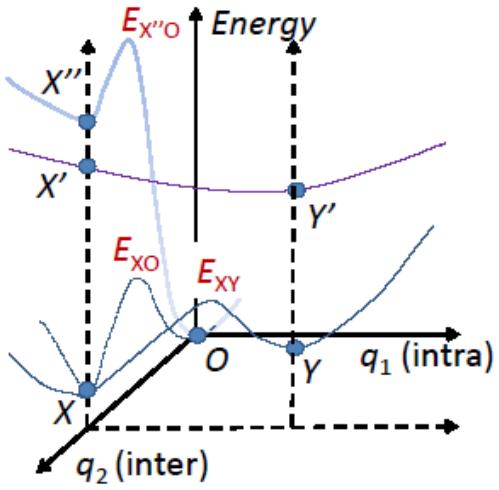

Fig. 5. Energy-configuration diagram for photodarkening (X-Y) and photo/thermal crystallization (X-O) (color online)

The diagram contains three ground states, O, X and Y. The origin O with a normalized energy denotes the lowest-energy, crystalline (trigonal) state. The point X assigns the quasi-stable amorphous state, in which Se chains are segmented and entangled with randomized dihedral angles [5-7], which makes inter-chain distances disordered. The energy E_x of the X state, which can be related with the residual entropy of 3.6 J/K•mol of a-Se [81], is estimated to be ~20 meV, which probably varies with Se chain lengths. And, the point Y represents the photo-darkened state, and accordingly, the energy difference E_{XY} may be comparable to the photodarkening magnitude of ~50 meV (Fig. 1) [16].

The three ground states are separated by energy barriers with heights E_B, which could be estimated as $\tau = \Omega^{-1}\exp(E_B/k_BT)$. Here, τ is a response time of $10^2 - 10^3$ s, Ω a typical vibrational frequency ~10^{12} /s, and T a related temperature. Regarding the barrier from X to O, the height E_{XO} corresponds to the crystallization temperature T_c. The barrier E_{XY} between X and Y could be estimated from annealing characteristics of the photodarkening just below T_g [16, 27]. Or, in terms of the bond-twisting model, the value is related with strained, bond-angular energy [18]. Besides, there could exist a barrier with a height E_{YO} (not shown), which may be comparable with E_c. However, since $T_g < T_c$, it seems difficult to estimate E_{YO} from thermal crystallization behaviours of photo-darkened samples.

Regarding the excitation energy, it is known that the photodarkening and the photo-crystallization are contrastive [4, 16, 27]. The photodarkening is maximally excited by Urbach-edge light of ~2.0 eV, the photon energy being located in the non-photoconducting gap, where localized, geminate electron-hole pairs are generated [4, 40]. By contrast, the photo-crystallization is efficiently induced by bandgap light of $\hbar\omega \geq 3.0$ eV [82], which is consistent with the observation [63] and predictions [52-54] that free holes contribute to the phenomenon. This spectral feature suggests that the photo-crystallization and the photoconduction, both being excited by bandgap

illumination, have one-to-one correspondence. Taking these observations into account, we locate two excited states X' and X'' above X, in which $E_{XX'} \approx 2.3$ eV and $E_{XX''} \approx 3.0$ eV (at 80 K), the values being likely to considerably (~ ±0.5 eV) scatter from site-to-site [40]. It is plausible that the transitions from X to X' and X'' are competitive, which may account for Roys' observation on suppression of the photo-crystallization by sub-gap illumination [83].

The temperature variations under illumination are also contrastive. The photo-crystallization characteristics [70, 71] suggest that the barrier energy $E_{X''O}$, which may be governed by crystallite growth, is higher than the energy corresponding to T_g. On the other hand, since the photodarkening becomes greater at lower temperatures [16], no energy barrier seems to exist in the geminate-pair state, which smoothly changes from X' to a polaronic state Y'. This structural transformation is assumed to be local, such as bond twisting [17, 18] and/or coordination exchange [11, 20, 21, 28], so that Y' is shifted from X' mainly along the intra-chain axis q_1. And, the polaronic geminate pair will recombine (non-)radiatively, relaxing to the quasi-stable state Y, giving rise to the photodarkening.

Table 2 lists calculated barrier heights. We see that all barrier heights are around ~1 eV, in accordance with other estimations [70, 71]; the result being ascribable to the fact that T_c is not very different from T_g. The energy is roughly a half of the bond energy of Se-Se of ~2 eV [4], which implies that thermal crystallization and glass transition occur through, not direct bond scission, but chain slippage and/or bond twisting [17, 18, 80].

Table 2. Energy barriers in Fig. 5, with T_g and T_c [5, 7]

Phenomenon, related barrier	Related temperature	Estimated barrier height
Thermal crystallization, E_{XO}	T_c ~ 390 K	~1.0
Photo-crystallization, $E_{X''O}$	$T_g \geq 310$ K	≥ 0.9 eV
Photodarkening, E_{XY}	$T_g < 310$ K	< 0.9 eV,

3.2. Vector changes

Table 1 shows that the vector effect could be divided into three levels; defective, extended, and oriented crystallization. And, for the first, Fritzsche proposed a phenomenological model [29, 34, 35], which can well explain the negative, photoinduced optical anisotropy. He assumes that linearly-polarized light selectively excites anisotropic elements having characteristic axes nearly parallel to the electric field, which will then *thermally* relax to varied directions, henceforth decreasing the optical activity parallel to the field. This idea can also explain the birefringence in As_2S_3 which is induced by illumination of unpolarized light that is incident upon sample sidewalls [29, 84]. A remaining problem is then the structural entity of the anisotropic element.

However, structural studies have confronted difficulties in determining the atomic structure. Comparing the scalar and vector photoinduced optical changes in As_2S_3, we estimate that the density of defective sites responsible for the optical anisotropy could be only ~0.1 at.% [4, 26], which is too few to be detected through structural studies [42, 43]. Besides, in a-Se, $r_2 \approx R \leq r_3$ (Table 3), where r_2 and r_3 are the second- and third-nearest intra-chain distance and R approximates the inter-chain distance. Accordingly, it is more-or-less difficult to detect chain alignments [60]. (Note that we are able to detect chain alignment in stretched polyethylene films [86, 87].)

Table 3. Comparisons of Se [4-7, 89] and polyethylene -(CH_2)- [81, 86, 87] in the intra-chain distances r_1, r_2, and r_3 with a typical interchain distance R [Å], the glass-transition temperature T_g [K], and the crystallization temperature T_c [K]

	r_1	r_2	r_3	R	T_g	T_c
Se	2.35	~3.7	3.5 ~ 5.8	~3.5	310	~390
polyethylene	~1.5	~2.5	3 ~ 4	~5	250	~410

On the other hand, several atomic pictures have been proposed for the anisotropic element [29, 30]. For instance, some researchers propose that the photoinduced anisotropy can be ascribed to orientational changes of valence-alternation pairs VAPs or intimate-VAPs [35, 88]. However, it seems difficult using the idea to interpret quantitative correspondences of the photoinduced birefringence and the natural birefringence in relevant crystals including Se and $As_2S(Se)_3$ [33]; the photoinduced birefringence in amorphous states is ~1/100 of the crystals; e.g. ~0.007 and ~0.8 in Se. Such an observation implies some resemblance of the photoinduced structure to the crystalline.

Under such circumstances, the photoinduced oriented crystallization that is demonstrated using x-ray diffraction and Raman-scattering spectroscopy unambiguously manifests that helical Se chains are responsible for the anisotropy [76-78]. Accordingly, it seems reasonable to assume that the optical anisotropy and the anisotropic deformation in amorphous states occur as pre-stages of the alignment of segmental chains; i.e., the optical anisotropy arises from local atomic orientation, which may be produced by photoinduced bond twisting [17, 18] and/or interchange [11, 20, 21, 28], and the anisotropic deformation seems to reflect two-dimensionally oriented chains (Fig. 6b), which are produced through extended-scale, domino-like chain alignments [45].

The latter idea is consistent with the parallel-to-E elongation [55, 58, 60] shown in Fig. 2. Neglecting bond angular effects and detailed interchain configurations, we approximate the atomic volume v in a-Se as $\sim rR^2$, where r (= r_1) and R represent the covalent length and the nearest-neighbour interchain distance (Table 3). Then, suppose that an amorphous sample consisting of N atoms and having a

cubic external shape with a side length of $(NrR^2)^{1/3}$, illustrated in Fig. 6a, is exposed to light having a vertical *E*. The Frizsche's idea suggests, taking dielectric anisotropy of Se chains into account [7, 33] and the photoinduced fluidity (Section 2.2), that in an ideal case the field rotates all segmental chains to horizontal directions, as in Fig. 6b, which will modify the sample shape to a rectangular parallelepiped with the bottom and vertical lengths of $N^{1/3}(rR)^{1/2}$ and $N^{1/3}R$. Then, such a configurational change of segments increases the *E*-parallel sample length with a ratio of $(R/r)^{1/3} \approx 1.14$, which is in quantitative agreement with the observed elongation of ~10% [58].

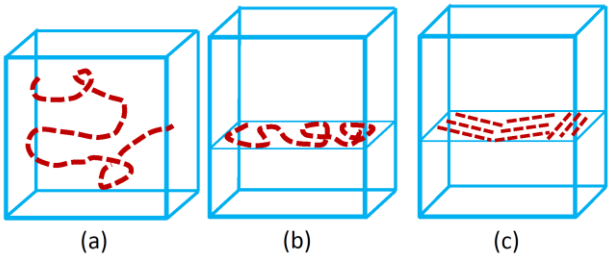

Fig. 6. Chain conformations in Se: (a) a three-dimensional disordered helix in a-Se before illumination, (b) and (c) are after illumination with a vertical E; (b) a two-dimensionally disordered helix and (c) a poly-crystalline structure with horizontal chain axes (photoinduced oriented crystallization). Note that the macroscopically cubic shape in (a) elongates in parallel to the E axis (vertical) in (b) and (c), under a fixed volume (color online)

Other anisotropic deformations could be understood as follows: the *E*-parallel M-shaped pattern in a-Se [48, 60], which appears upon illumination of focused (with diameters of ~10 μm) linearly-polarized light, is ascribable to the parallel elongation (Fig. 6) under Gaussian light-intensity distribution. The opto-mechanical effect, appearing also in a-Se [48] upon altering *E* direction, may be affected by the segmental alignment, in addition to optical forces [45]. On the other hand, the sample rotation shown in Fig. 2 could be triggered by optical torque [55].

4. Summaries

Amorphous Se is known to exhibit unique optical properties, i.e., efficient photoconductivity and many kinds of light-induced phenomena. The present work has comprehensively reviewed the latter topic, with a characteristic classification. A comparison of the phase change in Se with that in $GeSb_2Te_4$ is presented.

We also consider thermal crystallization, thermally-assisted photo-crystallization, and athermal photodarkening using a configuration-energy diagram. It contains some energy-minimal states and related barriers, the heights being estimated at ~1 eV, which reflects a rough relationship $T_g \approx T_c$; a characteristic probably being governed by the two-fold coordinated chain structure. Thermal structural relaxations could be connected with inter-chain conformation changes through chain slippage. Bond breakage could occur only under electronically-excited states, in which geminate and free carriers exert different effects.

Finally, a model for the photoinduced vector deformation has been proposed. The oriented crystallization manifests that the entity of anisotropic elements is segmental Se chains, so that it is straightforward to assume that other phenomena occurring in amorphous states could arise as pre-stages of chain orientation. The optical anisotropy is ascribable to defective bond alignment, and the vector deformation arises from two-dimensionally oriented fragments, which are produced through domino-like fluidic motions. However, the detection of anisotropic structures in amorphous states is challenging, since $r_2 \approx R$.

Acknowledgements

I would like to dedicate this work to Mihai Popescu in Romania, who passed away in 2019. As described by Lőrinczi et al. [90, 91], following Radu Grigorovici, he had performed enthusiastic studies on amorphous chalcogenide materials; publishing many papers, writing a text [1], and editing several volumes. In addition, he had stimulated related researches all over the world through organizing an international conference 'Amorphous and Nanostructured Chalcogenides, ANC' eight times from 2001 to 2017, and founding Ovshinsky Award [92]. He also appears to add a great contribution in publishing Journal of Optoelectronics and Advanced Materials, JOAM.

I myself have greeted him, with his wife Rodica, many times in international conferences in Bucharest and other places. I will never forget his gentle smile and continuous passion into chalcogenide materials.

References

[1] M. A. Popescu, Non-Crystalline Chalcogenides (Kluwer Academic Pub., Dordrecht, 2000).
[2] A.V. Kolobov (Ed.), Photo-Induced Metastability in Amorphous Semiconductors, (Wiley-VCH, Weinheim, 2003)
[3] M. Popescu, J. Optoelectron. Adv. M. **7,** 2189 (2005).
[4] K. Tanaka, K. Shimakawa, Amorphous Chalcogenide Semiconductors and Related Materials, 2nd Edition (Springer, Cham, 2021)
[5] P. Andonov, J. Non-Cryst. Solids **47**, 297 (1982).
[6] R. Brüning, E. Irving, G. LeBlanc, J. Appl. Phys. **89**, 3215 (2001).
[7] K. Tanaka, Springer Handbook of Glass, J. D. Musgraves, J. Hu, L. Calvez (Eds.): Ch. 19, Amorphous Selenium and Nanostructures (Springer, 2019).
[8] H. Hamanaka, Jpn. J. Appl. Phys. **13,** 1171 (1974).

[9] U. Vonwiller, Nature **104**, 347 (1919).
[10] R. Chang, Mat. Res. Bull **2**, 145 (1969).
[11] A.V. Kolobov, M. Kondo, H. Oyanagi, A. Matsuda, K. Tanaka. Phys. Rev. B **58**, 12004 (1998).
[12] K. Tanaka: J. Optoelectron. Adv. M. **15**, 1165 (2013).
[13] H. Koseki, T. Ueno, A. Odajima, Jpn. J. Appl. Phys. **17**, 1143 (1978).
[14] A. Roy, A.V. Kolobov, H. Oyanagi, K. Tanaka, Philos. Mag. B **78**, 87 (1998).
[15] Y. Sakaguchi, K. Tamura, Z. Phys. Chem. **235**, 189 (2021).
[16] K. Tanaka, A. Odajima, Solid State Commun. **43**, 961 (1982).
[17] K. Tanaka, J. Non-Cryst. Solids **59-60**, 925 (1983).
[18] K. Tanaka, Jpn. J. Appl. Phys. **25**, 779 (1986).
[19] R.T. Phillips, J. Non-Cryst. Solids **70**, 359 (1985).
[20] H. Koseki, A. Odajima, Jpn. J. Appl. Phys. **21**, 424 (1982).
[21] S.R. Elliott, J. Non-Cryst. Solids **81**, 71 (1986).
[22] K. Tanaka, Phys. Rev. B **30**, 4549 (1984).
[23] H. Ikemoto, T. Tsuzuki, M. Inui, M. Yao, H. Endo, Z. Phys. Chem. **216**, 1107 (2002).
[24] V. L. Averyanov, A. V. Kolobov, B. T. Kolomiets, V. M. Lyubin, Phys. Stat. Sol. A **57**, 81 (1980).
[25] A. Reznik, M. Klebanov, V. Lyubin, J. Appl. Phys. **105**, 013518 (2009).
[26] K. Tanaka, Phys. Status Solidi B **249**, 2019 (2012).
[27] A. Mishchenko, G. P. Lindberg, B. A. Weinstein, A. Reznik, Appl. Phys. Lett. **105**, 051912 (2014).
[28] J. Berashevich, A. Mishchenko, A. Reznik, Phys. Rev. Appl. **1**, 034008 (2014).
[29] K. Tanaka, Photoinduced anisotropy in chalcogenide glass, in Handbook of Advanced Electronic and Photonic Materials and Devices **5**, H.S. Nalwa (Ed.) (2001, Academic Press), Ch. 4, p. 119.
[30] V. M. Lyubin, M. L. Klebanov, Photo-induced anisotropy in chalcogenide glassy semiconductors, in Photo-Induced Metastability in Amorphous Semiconductors, A.V. Kolobov (Ed.), (2003, Wiley-VCH) Ch. 6, p. 91.
[31] V. G. Zhdanov, V. K. Malinovskii, Sov. Tech. Phys. Lett. **3**, 387 (1977).
[32] V. Lyubin, M. Klebanov, V. Tikhomirov, G. Adriaenssens, J. Non-Cryst. Solids **198-200**, 719 (1996).
[33] K. Tanaka, K. Ishida, N. Yoshida, Phys. Rev. B **54**, 9190 (1996).
[34] H. Fritzsche, J. Non-Cryst. Solids **164-166**, 1169 (1993).
[35] H. Fritzsche, Phys. Status Solidi B **246**, 1768 (2009).
[36] B. V. Deryagin, Yu. P. Toporov, K. I. Merzhanov, N. M. Galvidis, I. N. Aleinikova, L. N. Burta-Gopanovich, Sov. Phys. Solid State **16**, 1155 (1974).
[37] J.P. Larmagnac, J. Grenet, P. Michon, Philos. Mag. B **45**, 627 (1982).
[38] V. Palyok, I.A. Szabó, D.L. Beke, A. Kikineshi, Appl. Phys. A **74**, 683 (2002).
[39] M. Repka, M. Frumar, M. Hrdlicka, J. Phys. Chem. Solids **68**, 940 (2007).
[40] K. Tanaka, K. Shimakawa, J. Non-Cryst. Solids **481,** 579 (2018).
[41] V. V. Poborchii, A. V. Kolobov, K. Tanaka, Appl. Phys. Lett. **74**, 215 (1999).
[42] A.V. Kolobov, H. Oyanagi, K. Tanaka, Phys. Rev. Lett. **87,** 145502 (2001).
[43] H. Oyanagi, A. Kolobov, K. Tanaka, Intern. J. Modern Phys. B **16**, 1721 (2002).
[44] H. Hisakuni, K. Tanaka, Science **270**, 974 (1995).
[45] K. Tanaka, J. Non-Cryst. Solids **500**, 272 (2018).
[46] Y. Ikeda, K. Shimakawa, J. Non-Cryst. Solids **338–340**, 539 (2004).
[47] M. Popescu, F. Sava, A. Velea, I. -D. Simandan, K. Shimakawa, J. Non-Oxide Glasses **3**, 25, (2012).
[48] H. Asao, K. Tanaka, J. Appl. Phys. **102**, 043508 (2007).
[49] M. L. Trunov, P. M. Lytvyn, S. N. Yannopoulos, I. A. Szabo, S. Kökényesi, Appl. Phys. Lett. **99**, 051906 (2011).
[50] M. L. Trunov, P. M. Lytvyn, J. Non-Cryst. Solids **493**, 86 (2018).
[51] K. Tanaka, A. Saitoh, N. Terakado, J. Optoelectron. Adv. M. **8**, 2058 (2006).
[52] J. Hegedüs, K. Kohary, D.G. Pettifor, K. Shimakawa, S. Kugler, Phys. Rev. Lett. **95**, 206803 (2005).
[53] R. Lukács, J. Hegedüs, S. Kugler, J. Mater. Sci.: Mater. Electron. **20**, S33 (2009).
[54] K. Tanaka, J. Optoelectron. Adv. M. **19**, 586 (2017).
[55] K. Tanaka, N. Terakado, A. Saitoh, J. Optoelectron. Adv. M. **10**, 124 (2008).
[56] A. Saliminia, T. V. Galstian, A. Villeneuve, Phys. Rev. Lett. **85**, 4112 (2000).
[57] P. Krecmer, A. M. Moulin, R. J. Stephenson, T. Rayment, M. E. Welland, S. R. Elliott, Science **277**, 1799 (1997).
[58] K. Tanaka, M. Mikami, Phys. Status Solidi C **8**, 2756 (2011).
[59] K. Tanaka, Appl. Phys. Express **1**, 12006 (2008).
[60] K. Tanaka, M. Mikami, J. Non-Cryst. Solids **358**, 2385 (2012).
[61] K. Tanaka, N. Terakado, A. Saitoh, Phys. Status Solidi A **206**, 892 (2009).
[62] C. Lu, D. Recht, C. Arnold, Phys. Rev. Lett. **111**, 105503 (2013).
[63] J. Dresner, G.B. Stringfellow, J. Phys. Chem. Solids **29**, 303 (1968).
[64] R. Clement, J.C. Carballes, B. de Cremoux, J. Non-Cryst. Solids, **15** 505 (1974).
[65] L. Song, P. Galarneau, R. A. Lessard, Opt. Eng. **28**, 290 (1989).
[66] V. K. Tikhomirov, P. Hertogen, G. J. Adriaenssens, C. Glorieux, R. Ottenburgs, J. Non-Cryst. Solids **227–230**, 732 (1998).
[67] Q. Li, D. Qi, X. Wang, X. Shen, R. Wang, K. Tanaka, Jpn. J. Appl. Phys. **58,** 080911 (2019).
[68] A. A. Baganich, V. I. Mikla, D. G. Semak,

A. P. Sokolov, A. P. Shebani, Phys. Stat. Sol. B **166**, 297 (1991).
[69] S. N. Yannopoulos, J. Mater. Sci.: Mater. Electron. **31**, 7565 (2020).
[70] R. E. Tallman, B. A. Weinstein, A. Reznik M. Kubota, K. Tanioka, J. A. Rowlands, J. Non-Cryst. Solids **354**, 4577 (2008).
[71] R. E. Tallman, A. Reznik, B. A. Weinstein, S. D. Baranovskii, J. A. Rowlands, Appl. Phys. Lett. **93**, 212103 (2008).
[72] G. P. Lindberg, T. O'Loughlin, N. Gross, A. Mishchenko, A. Reznik, S. Abbaszadeh, K. S. Karim, G. Belev, B. A. Weinstein, J. Appl. Phys **116**, 193511 (2014).
[73] R. B. Stephens, J. Appl. Phys. **51**, 6197 (1981).
[74] I. F. Al-Hamarneh, B. N. Bulos, M. M. Abdul-Gader Jafar, J. Non-Cryst. Solids **355**, 305 (2009).
[75] E. V. Aleksandrovich, E. V. Stepanova, K. G. Mikheev, G. M. Mikheev, Tech. Phys. Lett. **44**, 797 (2018).
[76] K. Ishida, K. Tanaka, Phys. Rev. B **56**, 206 (1997).
[77] T. Innami, S. Adachi, Phys. Rev. B **60**, 8284 (1999).
[78] V. V. Poborchii, A. V. Kolobov, K Tanaka, Appl. Phys. Lett. **72**, 1167 (1998).
[79] N. Yamada, E. Ohno, K. Nishiuchi, N. Akahira, M. Takao, J. Appl. Phys. **69**, 2849 (1991).
[80] K. Tanaka, Solid State Commun. **34**, 201 (1980).
[81] L. Judovits, B. Wunderlich, J. Thermal Anal. **30**, 895 (1985).
[82] I. A. Paribok-Aleksandrovich, Sov-Phys. – Solid State **11,** 1631 (1970)
[83] A. Roy, A.V. Kolobov, K. Tanaka, J. Appl. Phys. **83**, 4951 (1998).
[84] K. Tanaka, M. Notani, H. Hisakuni, Solid State Commun. **95**, 461 (1995).
[85] K. Tanaka, Solid State Commun. **54**, 867 (1985).
[86] O. Yoda, I. Kuriyama, A. Odajima, J. Appl. Phys. **49**, 5468 (1978).
[87] G. R. Mitchell, R. Lovell, A. H. Windle, Polymer **23**, 1273 (1982).
[88] G. J. Adriaenssens, V. K. Tikhomirov, S. R. Elliott, J. Non-Cryst. Solids **227–230**, 688 (1998).
[89] J. Málek, R. Svoboda, Molecules **24**, 2725 (2019).
[90] A. Lőrinczi, P. Bădică, Toni Boţilă, M. Ciurea, A. Velea, A. Popescu, G. Socol, S. Antohe, N. Nedelcu, A. Sobetkii, Phys. Stat. Sol. B **257**, 2000284 (2020).
[91] A. Lőrinczi, Phys. Stat. Solidi B **257**, 2000142 (2020).
[92] M. Popescu, Phys. Stat. Solidi B **249**, 1835 (2012).

*Corresponding author: keiji@eng.hokudai.ac.jp